

# Polyoxometalate-Ionic Liquids for Mitigating the Effects of Iron Gall Ink Corrosion on Cellulosic Supports

Margarida Nunes, Pilar García-Orduña, Elena Atrián-Blasco, Joana Costa Vieira, Ana Paula Costa, Maria Emília Cabral Amaral, Ana Claro,\* Teresa Ferreira, and Scott G. Mitchell\*



Cite This: *ACS Omega* 2024, 9, 36609–36621



Read Online

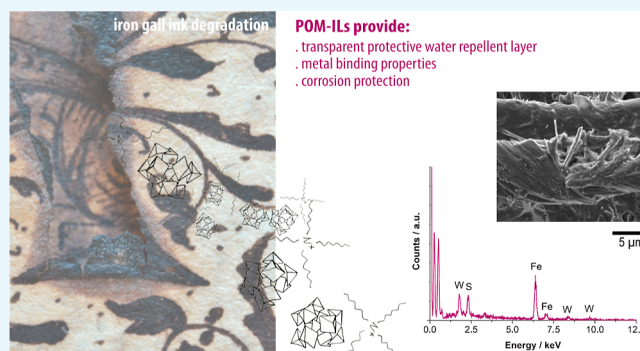
ACCESS |

Metrics & More

Article Recommendations

Supporting Information

**ABSTRACT:** Iron gall ink (IGI), renowned for its indelibility, was the most important writing ink in the Western world from the 15th to the late 19th century. However, it is now known that IGIs induce acid-catalyzed hydrolysis and iron-catalyzed oxidation of the cellulose in historical paper documents. These mechanisms of deterioration cause significant damage to the writing support materials, including color alteration and burn-through appearance, and in the worst scenarios, physical disintegration of the supports. Minimally invasive, long-term effective conservation treatments that tackle the underlying mechanisms of IGI degradation and their corrosion effects are yet to be developed. This study introduces the deployment of hydrophobic and anticorrosive polyoxometalate-ionic liquids (POM-ILs) as colorless coatings to counteract IGI-corrosion of cellulosic supports. Model IGI-containing papers (mockups) were prepared, coated with POM-ILs, and artificially aged to assess the compatibility of POM-ILs with IGI-containing documents. Comprehensive monitoring using colorimetric and scanning electron microscopy–energy-dispersive X-ray spectroscopy (SEM/EDS) analyses showed minimal interference with the aesthetic properties and morphology of the IGI mockups. In addition, polyoxometalates (POMs) with vacant metal atom sites in the cluster shell can be used to coordinate free transition metal ions. The ability of a monolacunary Keggin-type polyoxotungstate to coordinate free Fe(II) from IGI solution was demonstrated using UV–vis analysis. This led to the formation of a dimeric species,  $[(\text{SiW}_{11}\text{O}_{39}\text{Fe})_2\text{O}]K_{12}\cdot 28\text{H}_2\text{O}$ , which was characterized by single-crystal X-ray diffraction. Altogether, this study points to POM-ILs as promising protective coatings for effectively preserving historical IGI-written heritage.



## INTRODUCTION

The singular black color of varying hues and the indelibility of iron gall ink (IGI) have rendered it an essential part of Western writing practices since the 13th century.<sup>1,2</sup> Once idealized as a timeless favorite, it is now widely recognized that IGI poses a significant challenge to safeguarding our written cultural heritage. IGI action on cellulosic support can build up harmful decay phenomena on IGI-containing documents, such as color alteration, burn-through appearance, and embrittlement of the support, ultimately resulting in material loss.<sup>3–6</sup> Drawings by Leonardo da Vinci and Rembrandt van Rijn, cello suites composed by Bach, Isaac Newton's notes and letters from Charles Darwin, historical maps, and treatises on various topics, forming the groundwork of our contemporary knowledge are among the invaluable examples at risk of being lost forever due to the impact of IGI on cellulosic support.<sup>7–14</sup> Indeed, the formulation of the ink recipes plays a crucial role in the subsequent degradation processes, often hundreds of years later.

Numerous historical recipes for IGI are known, but the essential components included green vitriol (Fe(II) sulfate),

gallnut extracts, a source of polyphenolic (PPh)-rich compounds (e.g., tannic acid), and a water-soluble binder, typically Arabic gum.<sup>15</sup> Adding Fe(II) sulfate to gallnut extracts yields Fe(III)-PPh insoluble complex, responsible for the IGI color. Known recipes are predominantly unbalanced, featuring a surplus of Fe(II) sulfate over tannins.<sup>16</sup> Excess iron is a key factor in the IGI-corrosion process, potentiating the primary mechanisms responsible for cellulose degradation, i.e. acid-catalyzed hydrolysis and metal-catalyzed oxidation.<sup>17,18</sup> The former is primarily associated with the acidity of the ink, which promotes the hydrolytic scission of the  $\beta$ -(1,4)-glycosidic bonds responsible for linking the glucose units in the cellulose supramolecular structure.<sup>7,17,19</sup>

**Received:** May 25, 2024

**Revised:** July 2, 2024

**Accepted:** July 8, 2024

**Published:** August 18, 2024



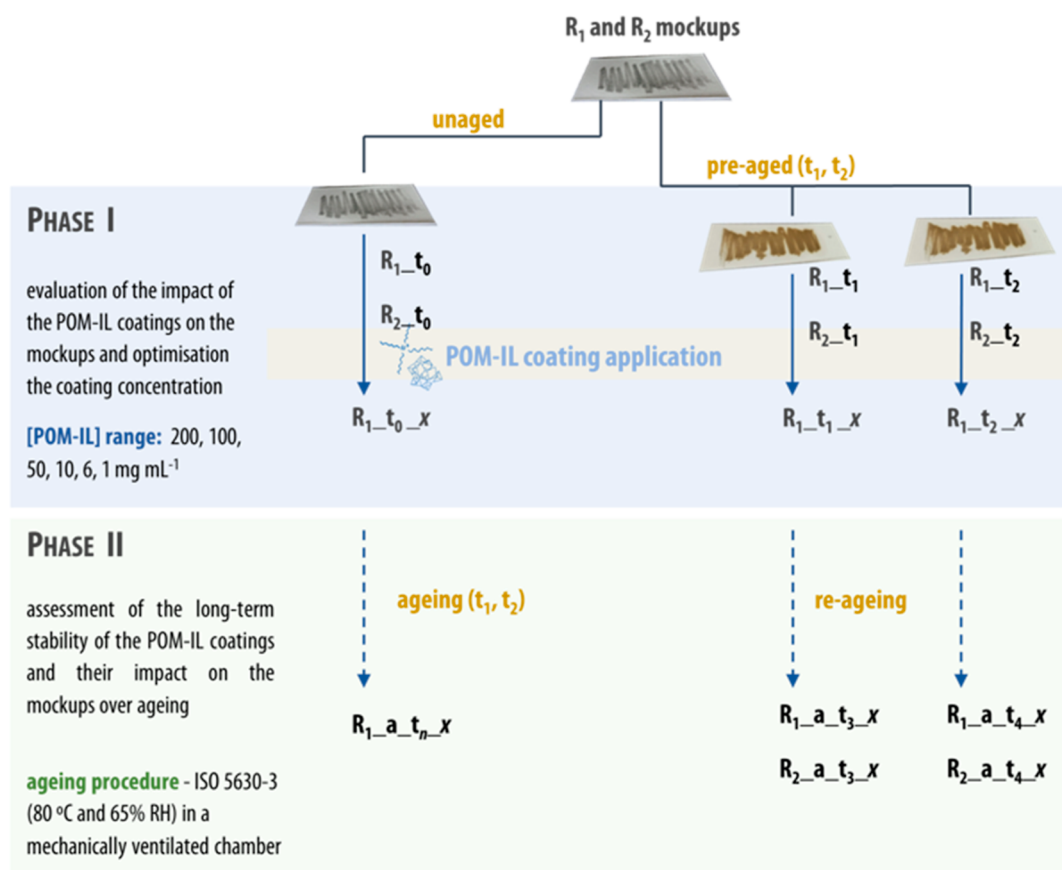


**Figure 1.** Overview of the experimental setup performed to study the impact and performance of the POM-IL coatings on the mockups. The samples were labeled according to the id in Table 1.

Fe(II) ions participate in Fenton and Fenton-like reactions, catalyzing the formation of reacting oxygen species, which can further participate in free radical chain processes (i.e., IGI-induced oxidation). In fact, it has been demonstrated that minimal amounts of Fe(II) are required to prompt the oxidation mechanism.<sup>20,21</sup>

Various conservation treatments have been developed and employed in the last decades to preserve IGI materials.<sup>11,22–25</sup> According to the literature, appropriate treatments able to attenuate the IGI effects on paper require two processes—deacidification and inactivation of free transition metal ions, principally Fe(II).<sup>7,26,27</sup> The so-called “calcium phytate method” was introduced by Neevel<sup>16</sup> for IGI-degraded documents. Proven effective as an alkaline aqueous treatment, it became a standard option within the IGI context. Phytate is an effective chelator of divalent cations [e.g., Fe(II), Cu(II)], preventing iron ions from remaining free to participate in the degradation mechanisms prompted by IGI (i.e., acid-hydrolysis and metal-catalyzed oxidation of cellulose).<sup>8,28</sup> While effective in counteracting IGI-induced degradation on cellulosic support, this treatment falls short in limiting crucial effects like the embrittlement and physical disintegration of the support. Furthermore, some authors<sup>3,28,29</sup> emphasize the need for caution when relying on alkali solutions for deacidification treatments of IGI-containing documents. The basicity of these solutions can promote an array of unwanted side effects, including ink lateral migration, ink color changes, and physical degradation of the cellulosic support.<sup>28,29</sup> Besides, paper deacidification by aqueous solutions is unsuitable for water-sensitive paper-based items. Nonaqueous alternatives have

then emerged as alternatives.<sup>22,26,30,31</sup> Rouchon et al.<sup>31</sup> introduced an approach that sets aside the aqueous treatment using interleaves charged with halide compounds, such as calcium or sodium bromide, also known as the “interleaving technique”. The concept involves sandwiching IGI-containing documents between those leaves, facilitating the halide compounds to migrate to the documents. This process decreases acidity, delaying paper decay.<sup>26,31</sup> The authors achieved promising results while observing minimal lateral and transversal ink migration.

With all this in mind, sustainable conservation-oriented IGI research should ideally be based on three key points: minimal invasiveness, negligible side effects, and long-term mechanical and chemical stabilization.

We hypothesized that innovative conservation treatments based on the use of hydrophobic Polyoxometalate-Ionic Liquids (POM-ILs) possessing anticorrosive and metal-chelating properties could help to mitigate the long-term deleterious effects of IGI degradation on cellulosic support. Polyoxometalates (POMs for short) are a prominent and diverse class of nanoscale molecular metal-oxide clusters typically constructed from W, Mo, or V (in their highest oxidation states) surrounded by oxygen atoms as ligands.<sup>32</sup> Combining a POM anion of choice with a bulky organocation, such as a quaternary ammonium or phosphonium cation, can lead to versatile POM-IL materials.<sup>32,33</sup> Multifunctional POM-ILs retain many of the key properties of the discrete cationic and anionic species and can, therefore, be chemically tuned by separate modifications of each component. POM-ILs are being increasingly studied in various fields due to their redox

properties, high oxidation activity, and antimicrobial protection; thus, several applications have been developed in the past few years, including for conservation and restoration.<sup>32,34–36</sup> Franco-Castillo et al.<sup>36,37</sup> have recently contributed to using POM-ILs to safeguard built cultural heritage from microbial colonization. For example, the authors conducted a study to limit the growth of lampenflora on chalk substrates exploring two POM-ILs prepared by using a Keggin-type anion,  $[\alpha\text{-SiW}_{11}\text{O}_{39}]^{8-}$ , and two different tetraalkylammonium ions (tetraheptylammonium and trihexyl tetradecyl ammonium). The results have demonstrated that POM-ILs exhibit more effective antimicrobial performance than the widely used cleaning agent Preventol RI80 against two specific algal strains growing on the bas-reliefs carved in the underground Pommery Champagne Cellar in Reims (France).<sup>37</sup> A crucial achievement was to assess the above-mentioned performance with low-concentration colorless coatings. Since one of the main concerns in conservation treatments is their potential to cause color alterations, using colorless coatings is critical. Recently, the same authors<sup>37</sup> evaluated the efficacy of POM-ILs on natural calcareous stones under simulated weathering conditions and in real outdoor environments. Overall, POM-ILs were determined to be suited to deployment as preventative biocidal coatings for porous and nonporous stones. However, the coatings affected the microstructural porosity of the porous stones, indicating that optimal concentrations of the solutions are required to provide the correct balance between biocidal protection and maintaining the natural properties of the stones. Additionally, the potential of POM-ILs for protecting against metal corrosion has been successfully demonstrated.<sup>32,36</sup>

Therefore, it stands to reason that POM-ILs with synergistic properties could, in principle, be tailored to meet the requirements for preventing or mitigating IGI corrosion on cellulosic materials. We aimed to study the ability of POM-IL to chelate free Fe(II) ions and evaluate how colorless POM-IL solutions can be applied as protective coatings that do not interfere with the aesthetic properties of the paper documents. This research has the potential to shed light on new possibilities for more convenient handling and processing to protect IGI-written heritage effectively.

## ■ EXPERIMENTAL DESIGN

This work was conducted in a two-phase procedure (I and II), graphically depicted in Figure 1. POM-ILs were synthesized and applied on IGI-containing cellulosic model samples (mockups) to evaluate the impact of the POM-ILs on cellulosic support over artificial aging and their effectiveness in counteracting IGI-corrosion. The procedures and methodology are briefly explained below, with comprehensive information available in the Supporting Information.

The materials, synthesis procedures and characterization of the POM, Fe-substituted POM, and POM-ILs are available in Supporting Information, Section 1. In addition, the mockup preparation and the artificial aging procedures are briefly explained in Supporting Information Section 2 and detailed elsewhere.<sup>38</sup> The application procedure of POM-ILs on the mockups is also available (Supporting Information, Section 3). The analytical instrumentation used, including color and pH measurements, scanning electron microscopy/energy-dispersive X-ray spectroscopy (SEM/EDS), Fourier transform infrared–attenuated total reflectance (FT-IR-ATR) analysis,

physical tests, and corresponding experimental conditions, is also detailed in Supporting Information (Section 4).

**Mockups Preparation and Artificial Aging.** The mockups were prepared by brushing or writing two distinct IGI reproductions ( $R_1$  and  $R_2$ , detailed in Table S1) on the Whatman paper (Table S2). The application modes (brushing vs writing) aimed to simulate painted areas in historical documentation and conventional writing, respectively. Different sets of mockups were prepared for the characterization and physical tests, each comprising a variable number of sheet strips in various sizes. Before applying POM-ILs, an artificial aging procedure was performed on a set of mockups. The samples were identified as “unaged” ( $t_0$ ) and “pre-aged” mockups ( $t_n$ ,  $n = 1$  and  $2$ , to indicate four- and five-week aging, respectively) (Table S3). Unaged mockups represent a fresh model sample, while pre-aged mockups are intended to simulate typical historical documents.

**POM-IL Coatings Preparation, Application, and Re-aging Procedure.** POM-IL 1 and 2 were synthesized according to the procedure described in Supporting Information (Section 1). Briefly, POM-ILs 1 and 2 were prepared using the lacunary Keggin polyoxoanion  $[\alpha\text{-SiW}_{11}\text{O}_{39}]^{8-}$ , and tetraheptylammonium bromide (POM-IL 1) and trihexyltetradecylammonium bromide (POM-IL 2). These highly viscous POM-ILs were diluted in acetone at concentrations of 200, 100, 50, 10, 6, and 1 mg mL<sup>-1</sup>. The most concentrated dilutions (200 and 100 mg mL<sup>-1</sup>) exhibited a yellowish appearance, whereas the solutions with lower concentrations were colorless and transparent (Figure 3a).

In order to evaluate the impact of the POM-ILs on  $R_1$  and  $R_2$  mockups and optimize the concentration of the coatings, each solution of POM-IL was brushed on the unaged and pre-aged mockup surfaces (Figure 1 and Tables S4 and S5). The volume of POM-IL coatings applied per mockup varied according to their size. The coatings were brushed with a Da Vinci 374 flat painting brush no. 0, with a 1–2 min gap between applications to allow for proper air-drying. Subsequently, the coated mockups were placed on a desk and carefully covered with a dark surface for 24 h to ensure effective drying and avoid light interaction and contaminations. A comprehensive characterization of these samples was conducted before coating application and at one and 30 days after the application. After the 30 day period, the mockups were kept in a dark room at room temperature.

Additionally, to assess the long-term stability of the coatings and their impact on the mockups over aging (phase II, Table S5), we selected the mockups coated with the 100 mg mL<sup>-1</sup> POM-IL solution and subjected them to an artificial aging procedure conducted according to the ISO 5630-3.<sup>39</sup> Hence, two aging periods were defined for the unaged coated mockups: four and five weeks, labeled as  $t_1$  and  $t_2$ , respectively. Sets of 12 mockups (six brushed and six written) were removed at each aging period. The pre-aged, coated mockups were subjected to a one-week re-aging procedure under similar aging conditions. The samples were labeled according to the identification codes (id) detailed in Table 1. An overview of the experimental setup employed is illustrated in Figure 1.

## ■ RESULTS AND DISCUSSION

**Mockups Characterization.** We established the groundwork for this research in our previous work,<sup>38</sup> where we comprehensively characterized the IGI reproductions ( $R_1$  and  $R_2$ ) and the mockups. In the Supporting Information (Section

**Table 1. Sample Codes, Ageing and Coating Conditions, and Observations<sup>a</sup>**

	samples id	aging conditions	coating conditions	observations
phase I	R <sub>1</sub> w_t <sub>0</sub>	unaged mockups	uncoated	control
	R <sub>1</sub> b_t <sub>0</sub>			
	R <sub>2</sub> w_t <sub>0</sub>			
	R <sub>2</sub> b_t <sub>0</sub>			
	R <sub>1</sub> w_t <sub>0_x</sub>	unaged mockups	coated	
	R <sub>1</sub> b_t <sub>0_x</sub>			<i>x</i> = 1 (POM-IL1)
	R <sub>2</sub> w_t <sub>0_x</sub>			<i>x</i> = 2 (POM-IL2)
	R <sub>2</sub> b_t <sub>0_x</sub>			
	R <sub>1</sub> w_t <sub>n</sub>	pre-aged mockups	uncoated	control
	R <sub>1</sub> b_t <sub>n</sub>			
R <sub>2</sub> w_t <sub>n</sub>	pre-aged mockups	coated	<i>n</i> = 1 (4 weeks)	
R <sub>2</sub> b_t <sub>n</sub>			<i>n</i> = 2 (5 weeks)	
R <sub>1</sub> w_t <sub>n_x</sub>			<i>n</i> = 1 (4 weeks)	
R <sub>1</sub> b_t <sub>n_x</sub>			<i>n</i> = 2 (5 weeks)	
R <sub>2</sub> w_t <sub>n_x</sub>			<i>x</i> = 1 (POM-IL1)	
R <sub>2</sub> b_t <sub>n_x</sub>			<i>x</i> = 2 (POM-IL2)	
phase II	R <sub>1</sub> w_a_t <sub>n_x</sub>	aged mockups	coated	<i>n</i> = 1 (4 weeks)
	R <sub>1</sub> b_a_t <sub>n_x</sub>			<i>n</i> = 2 (5 weeks)
	R <sub>2</sub> w_a_t <sub>n_x</sub>	re-aged mockups	uncoated	<i>x</i> = 1 (POM-IL1)
	R <sub>2</sub> b_a_t <sub>n_x</sub>			<i>x</i> = 2 (POM-IL2)
	R <sub>1</sub> w_a_t <sub>n</sub>			control
	R <sub>1</sub> b_a_t <sub>n</sub>			<i>n</i> = 3 ( <i>t</i> <sub>1</sub> + 1 week)
	R <sub>2</sub> w_a_t <sub>n</sub>			<i>n</i> = 4 ( <i>t</i> <sub>2</sub> + 1 week)
	R <sub>2</sub> b_a_t <sub>n</sub>			
	R <sub>1</sub> w_a_t <sub>n</sub>	re-aged mockups	coated	
	R <sub>1</sub> b_a_t <sub>n</sub>			<i>n</i> = 3 ( <i>t</i> <sub>1</sub> + 1 week)
R <sub>2</sub> w_a_t <sub>n</sub>	<i>n</i> = 4 ( <i>t</i> <sub>2</sub> + 1 week)			
R <sub>2</sub> b_a_t <sub>n</sub>				

<sup>a</sup>R<sub>1</sub>, R<sub>2</sub>—ink reproductions (see Table S1); b—brushed; w—written; a—artificial aging; t<sub>n</sub>—aging period; x—POM-IL coating.

5), we summarized the mockups characterization results. For simplicity and given that the following discussion primarily centers on the R<sub>1</sub>b mockups, only the key results of the characterization of this sample will be presented.

#### Validating the Ability of POMs to Coordinate Iron.

Single crystals were obtained by adding iron sulfate to the Keggin-type POM K<sub>8</sub>[α-SiW<sub>11</sub>O<sub>39</sub>] as described in Supporting Information Section 1. The single crystal structure of the obtained dimeric compound [(SiW<sub>11</sub>O<sub>39</sub>Fe)<sub>2</sub>O]<sup>12-</sup> is illustrated in Figure 2, and the selected geometrical parameters and the crystallographic data and structural refinement parameters are detailed in Tables 2 and 3.

The compound crystallizes in a triclinic  $\bar{P}1$  space group and has the empirical formula [(SiW<sub>11</sub>O<sub>39</sub>Fe)<sub>2</sub>O]K<sub>12</sub>·28H<sub>2</sub>O (Table 3). Specifically, the dimeric compound contains two [(SiW<sub>11</sub>O<sub>39</sub>Fe)<sub>2</sub>O]<sup>12-</sup> polyoxoanion subunits linked by a Fe—

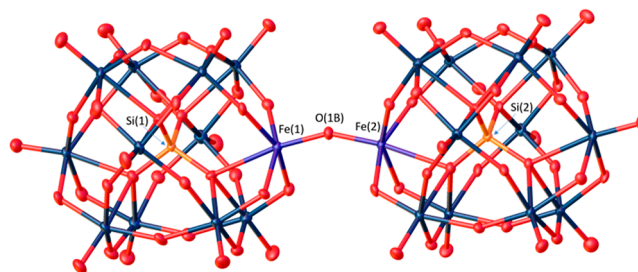


**Figure 2.** Molecular structure (ellipsoid representation at 50% probability level) of dimeric [(SiW<sub>11</sub>O<sub>39</sub>Fe)<sub>2</sub>O]<sup>12-</sup>. For clarity, only selected atoms have been labeled. Color scheme: O—red; Fe—purple; Si—orange; and W—blue.

**Table 2. Selected Bond Lengths (Å) and Angles (deg) in [(SiW<sub>11</sub>O<sub>39</sub>Fe)<sub>2</sub>O]K<sub>12</sub>·28H<sub>2</sub>O<sup>a</sup>**

bond	bond lengths
Fe(1)—O(1B)	1.800(7)
Fe(2)—O(1B)	1.794(7)
Fe(1)—O(1B)—Fe(2)	154.0(5)
Fe(1)...O(2I)	2.409(8)
Fe(2)...O(5I)	2.448(7)
range; mean value ( $\bar{x}$ )	
Fe—O <sub>w</sub> <sup>a</sup>	1.986(8)—2.023(8); $\bar{x}$ = 2.006(2)
W—O <sub>w2</sub> <sup>a</sup>	1.837(7)—2.030(8); $\bar{x}$ = 1.9251(8)
W—O <sub>t</sub> <sup>b</sup>	1.701(8)—1.733(8); $\bar{x}$ = 1.7153(1)
W—O <sub>i</sub> <sup>c</sup>	2.288(7)—2.340(6); $\bar{x}$ = 2.3369(1)
Si—O <sub>i</sub> <sup>c</sup>	1.616(8)—1.634(8); $\bar{x}$ = 1.627(2)

<sup>a</sup>O(1B)—bridging O between Fe atoms; O<sub>w</sub>—O atoms bonded to Fe and W; O<sub>w2</sub>—O atoms bonded to two W atoms; O<sub>i</sub>—O atoms bonded to Si and three W atoms (inside the cage); O<sub>t</sub>—terminal O atoms, bonded only to one W atom; <sup>b</sup>t—terminal O; <sup>c</sup>i—insider O.

O—Fe bridge. These two subunits have the conventional alpha Keggin structure composed of edge-sharing WO<sub>6</sub> distorted octahedra and a central silicon atom surrounded by an ordered tetrahedral arrangement of four oxygen atoms. A full summary of the bond lengths and angles is available in the Supporting Information file (Table S7). Iron atoms have distorted octahedral coordination environments formed by six oxygen atoms: the equatorial coordination plane defined by four bridging oxygen atoms (bound to tungsten atoms), while axial positions are occupied by an oxygen from the SiO<sub>4</sub> tetrahedral central unit and another from the μ-O bridge (O1B atom). Iron—oxygen bond lengths ranging from 1.986(8) to 2.023(8) Å in the equatorial plane, and Fe—O axial bond lengths in Fe—O—Fe bridge [1.800(7) and 1.794(7) Å], well agree with those found in [(PW<sub>11</sub>O<sub>39</sub>Fe)<sub>2</sub>O]<sup>10-</sup> related fragment.<sup>40</sup> On the contrary, internal Fe—O axial bond lengths between iron atoms and closer oxygen atoms from the SiO<sub>4</sub> core [2.409(8) and 2.448(7) Å] have been found to be shorter than those found in the PO<sub>4</sub>-containing compound [2.564(5) and 2.590(6)] Å.<sup>40</sup>

The features of the almost linear Fe—O—Fe bridge [with a 154.0(5)° angle, leading to a Fe...Fe intermolecular distance of 3.502(2) Å] are in agreement with the ones reported for dimeric μ-oxo bridged Fe complexes.<sup>41,42</sup> Table 2 presents the selected bond lengths (Å) and angles (deg) in [(SiW<sub>11</sub>O<sub>39</sub>Fe)<sub>2</sub>O]K<sub>12</sub>·28H<sub>2</sub>O.

Thermogravimetric and FT-IR analysis (see Supporting Information Section 4) were conducted to characterize the [(SiW<sub>11</sub>O<sub>39</sub>Fe)<sub>2</sub>O]K<sub>12</sub>·28H<sub>2</sub>O. The FT-IR spectrum (Figure S2) shows the characteristic bands of the Fe-substituted

**Table 3. Crystal Data and Structure for  $[(\text{SiW}_{11}\text{O}_{39}\text{Fe})_2\text{O}]_{\text{K}_{12}}\cdot 28\text{H}_2\text{O}$** 

empirical formula	$[(\text{SiW}_{11}\text{O}_{39}\text{Fe})_2\text{O}]_{\text{K}_{12}}\cdot 28\text{H}_2\text{O}$
formula weight	6450.23
temperature (K)	100(2)
wavelength (Å)	0.710731
crystal system	triclinic
space group	$P\bar{1}$
<i>a</i> (Å)	13.4690(7)
<i>b</i> (Å)	19.7413(10)
<i>c</i> (Å)	20.2551(10)
$\beta$ (deg)	79.120(2)
$\alpha$ (deg)	67.751(2)
$\gamma$ (deg)	88.382(2)
volume (Å <sup>3</sup> )	4889.6(4)
<i>Z</i>	2
absorption coefficient (mm <sup>-1</sup> )	26.705
min and max transmission factors	0.0251, 0.1224
completeness to $\theta_{\text{max}}$ (%)	99.9
refinement method	full-matrix least-squares on $F^2$
data/restraints/parameters	24256/0/1111
goodness-of-fit on $F^2$	1.155
$F(000)$	5696
crystal size (mm)	0.060 × 0.065 × 0.180
reflections collected/unique	385466/24258 [ $R(\text{int}) = 0.0645$ ]
<i>R</i> indices [ $I > 2\sigma(I)$ ]	$R1 = 0.0444$ ; $wR2 = 0.1061$ [23417 ref]
<i>R</i> indices (all data)	$R1 = 0.0457$ ; $wR2 = 0.1069$
largest diff. peak and hole (e/Å <sup>3</sup> )	8.53/−3.67

Keggin POM, particularly in the region between 600 and 1000  $\text{cm}^{-1}$ . The wavenumber region below 1000  $\text{cm}^{-1}$  is characteristic of the W–O stretching and bending vibrations and the corresponding bands were observed at *ca.* 958  $\text{cm}^{-1}$  [ $\nu_{\text{as}}(\text{W}-\text{O}_t)$ ], 892  $\text{cm}^{-1}$  [ $\nu_{\text{as}}(\text{W}-\text{O}_b-\text{W})$ ], and 789  $\text{cm}^{-1}$  [ $\nu_{\text{as}}(\text{W}-\text{O}_a-\text{W})$ ] (where  $\text{O}_t$  = terminal oxygen,  $\text{O}_b$  = bridging oxygen,  $\text{O}_a$  = internal oxygen). In addition, the bands at 789 and 715  $\text{cm}^{-1}$  are typical of  $\nu_{\text{as}}(\text{Fe}-\text{O}-\text{Fe})$  of dimeric polyoxotungstate,<sup>43</sup> evidencing the existence of a dimeric structure,<sup>44</sup> and the band at 518  $\text{cm}^{-1}$  was assigned to Fe–O vibrations (Table S8). Similar results were reported by Kuznetsova<sup>45,46</sup> while investigating the structure and catalytic properties of transition metal (e.g., iron) complexes with heteropolyanions, and more recently, Xue et al.<sup>44</sup> assessed similar data when studying the structural transformation of dimeric mono-Fe(III)-substituted Keggin-type polyoxotungstates. These results support our hypothesis, confirming the POM ability to coordinate Fe.

After validating the ability of the POMs to coordinate iron, UV–vis spectroscopy was carried out to study their effectiveness in retrieving Fe(II) ions from an IGI solution. The UV–vis spectra of IGI, POM and the prepared POM-IGI solution are shown in Figure S3. IGI showed a typical spectrum with a band at *ca.* 248 nm and *ca.* 590 nm associated with the IGI complex.<sup>47</sup> After adding the POM to the IGI solution, one can infer that the formation of the Keggin-type Fe(II)-substituted from  $\text{K}_8[\alpha\text{-SiW}_{11}\text{O}_{39}]$  occurred immediately by the emergence of the band at *ca.* 256 nm (O → W charge transfer) and a shoulder *ca.* 330 nm (O → Fe charge transfer).<sup>40,48</sup> Hence, the ability of the POM to coordinate Fe(II) was attested. This aspect holds paramount significance due to the implications associated with the presence and penetration of Fe(II) ions within the cellulosic structure in IGI-containing documents. As previously explained, free Fe(II)

ions facilitate the occurrence of acid hydrolysis by increasing the acidity of the IGI-cellulose system. This phenomenon was attested by Rouchon and Bernard<sup>19</sup> and more recently by Gimat et al.<sup>25</sup> Besides, Fe(II) ions play a key role in the well-known Fenton reactions, forming reactive radicals which catalyze cellulose oxidation. Importantly, our previous work<sup>38</sup> showed that oxidation seems to be the driving mechanism of cellulose degradation.

In a similar approach but in the context of Alzheimer's disease, Atrián-Blasco<sup>48</sup> demonstrated the ability of Keggin-type POMs to coordinate Cu(II) from Cu(II) (Amyloid- $\beta$ ). The authors reported the formation of  $[\alpha\text{-SiW}_{11}\text{O}_{39}\text{Cu}(\text{OH}_2)]^{6-}$  anion from the monolacunary,  $[\alpha\text{-SiW}_{11}\text{O}_{39}]^{8-}$  in the presence of Cu(II) through the emergence of a band at *ca.* 253 nm in the UV–vis spectrum. Our findings are commensurate with those reported by the authors.<sup>48</sup> Besides, the smooth shoulder found at *ca.* 590 nm in the POM-IGI spectrum serves as an indicator of the effective removal of Fe(II) from the solution by the POM. According to Santos et al.<sup>40</sup> this feature might be associated with the ligand field transitions that gain intensity either by mixing with the intense near-UV O → Fe charge transfer or by an exchange mechanism. Interestingly, this result suggests a bent of Fe–O–Fe geometry, which aligns with our crystallographic data.

## PHASE I—CHARACTERIZING THE IMPACT OF THE POM-IL COATINGS ON THE MOCKUPS

### Visual Examination and Evaluation of Color and pH.

Overall, visual examination of the mockups coated with the POM-ILs indicated minimal aesthetic alterations regarding the uncoated mockups (Figure 3b). The more pronounced alterations were observed for the mockups coated with the 200  $\text{mg mL}^{-1}$  coating solutions, particularly in those where

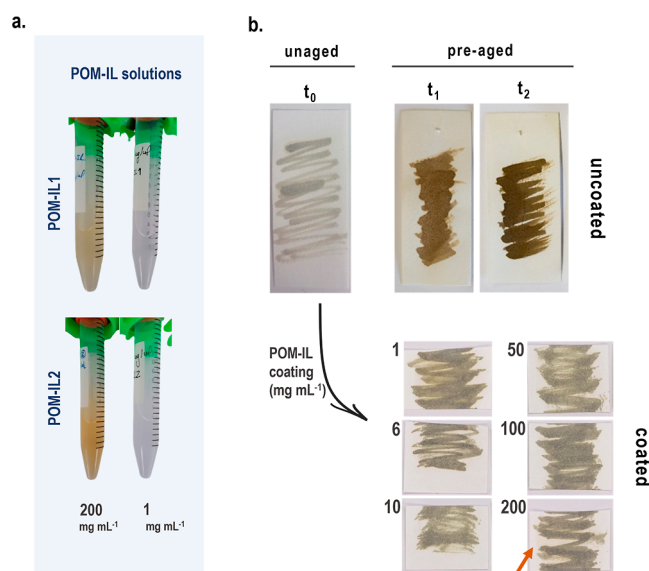


**Figure 3.** (a) Representative images of the POM-IL solutions at the highest and lowest concentrations (200 and 1  $\text{mg mL}^{-1}$ , respectively); (b) Representative uncoated  $R_1$  mockups [unaged and pre-aged ( $t_1$  and  $t_2$ )] and the unaged corresponding coated mockups with POM-IL2 coatings (concentration range from 1 to 200  $\text{mg mL}^{-1}$ ). An orange arrow highlights the mockup coated with the most concentrated coating (POM-IL2 at 200  $\text{mg mL}^{-1}$ ), which displayed minor aesthetic alterations, i.e. visible yellowish coating reminiscent of fatty substances occurring on the cellulosic support.

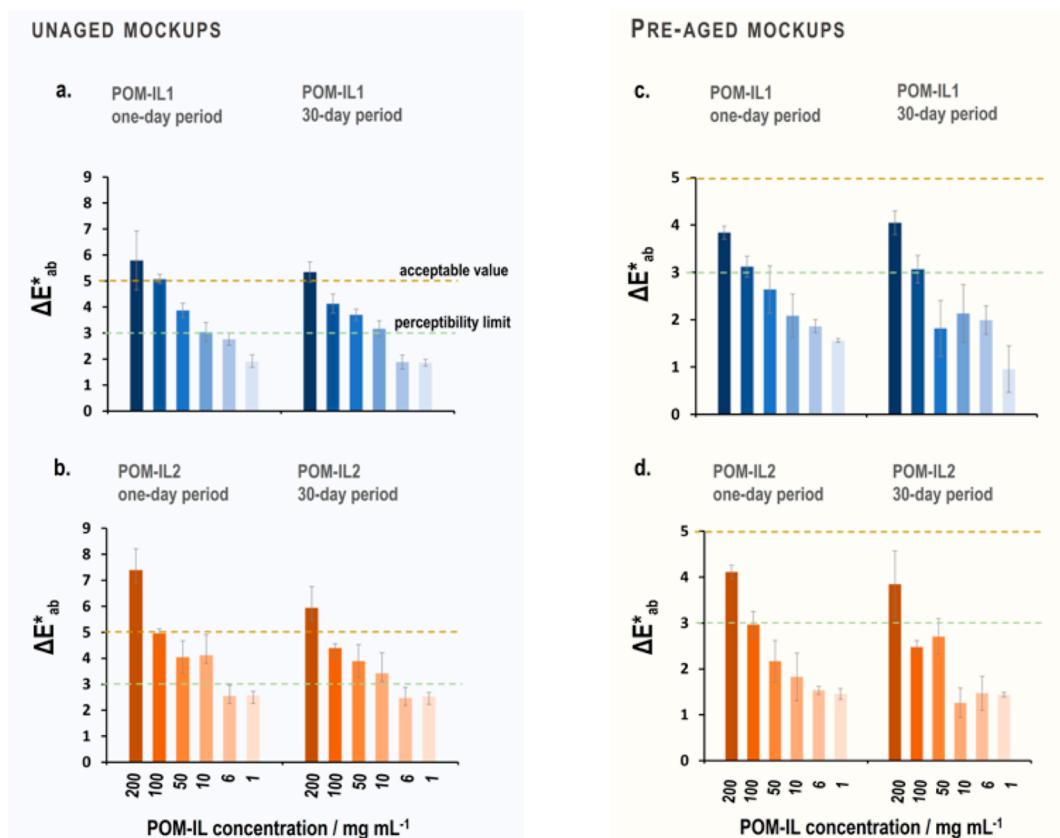


**Figure 4.** Color variation ( $\Delta E_{ab}^*$ ) estimated between: (a,b) the unaged mockups ( $R_{1b\_t_0}$ ) coated with POM-IL1 and POM-IL2, respectively, and their corresponding uncoated; (c,d) pre-aged mockups ( $R_{1b\_t_1}$ ) coated with POM-IL1 and POM-IL2, respectively, and their corresponding uncoated mockups.

POM-IL2 were used. Similar observations were found for the pre-aged, coated mockups.

Colorimetric analyses were conducted to evaluate the color changes caused by applying the POM-ILs on the mockups. Since similar trends were verified for the brushed and written mockups, regardless of the ink reproduction ( $R_1$  or  $R_2$ ), for simplicity, the CIELab discussion focuses solely on the  $R_{1b}$  mockups results (i.e., mockups prepared with  $R_1$  ink by the brushing method). The remaining results can be found in [Supporting Information](#) (Tables S9–S11 and Figures S4 and S5). Variation of the  $L^*a^*b^*$  coordinates ( $\Delta L^*$ ,  $\Delta a^*$ , and  $\Delta b^*$ ) (Figure S4) and color variation ( $\Delta E_{ab}^*$ ) (Figure 4) were estimated for the unaged and pre-aged mockups, before ( $R_{1b\_t_0}$ ;  $R_{1b\_t_n}$ , respectively) and upon applying the POM-IL coating ( $R_{1b\_t_0\_x}$ ;  $R_{1b\_t_n\_x}$ ). This evaluation was performed one day (to allow the coating to dry effectively) and 30 days following the application of the coatings.

One day after coating, the  $R_{1b\_t_0\_1}$  mockup exhibited a shift toward darker brownish colors, primarily due to a decrease in the  $L^*$  coordinate ( $\Delta L^* < 0$ ), along with an overall increase in the yellow coordinate ( $\Delta b^* > 0$ ) (Table S9 and Figure S4). The estimated alterations were more pronounced for the 200 and 100 mg mL<sup>-1</sup> POM-IL1-coated mockups. The increase observed for the  $b^*$  coordinate to more positive values showed that POM-IL1 coating, particularly solutions between 200 and 50 mg mL<sup>-1</sup>, tended to alter the yellowish hue of the mockups slightly. Limited alterations were observed for the  $a^*$  coordinate regardless of the POM-IL1 concentration. Similar results, within the error, were determined for POM-IL2 coating. However, the mockups exhibited more yellowing

when coated with POM-IL2, likely attributed to the honey-yellow color of this solution.

In sum, the color alterations of the mockups induced by the POM-IL coatings were observed as an overall darkening and yellowing of the samples, predominant in the mockups coated with the more concentrated solutions.

Interestingly, the color coordinates tended to stabilize over time, returning to values more proximal to the starting values. Figure 4a,b displays the  $\Delta E_{ab}^*$  for phase I, consisting of the unaged mockups ( $R_{1b\_t_0}$  vs  $R_{1b\_t_0\_x}$ ) coated with POM-IL1 and POM-IL2 both one-day (left) and 30 day (right) period after the application. As expected, the  $\Delta E_{ab}^*$  of the mockups tend to alter depending on the concentrations of POM-IL coatings. When evaluating the  $\Delta E_{ab}^*$  of the mockups 1 day after applying the POM-IL1 coating (Figure 4a, left), larger values were found for the mockups coated with the solutions of higher concentrations (i.e.,  $\Delta E_{ab}^*$  of  $5.8 \pm 1.1$ ,  $5.1 \pm 0.2$ ,  $3.9 \pm 0.3$  CIELab units for 200, 100, 50 mg mL<sup>-1</sup> solutions, respectively). Nevertheless, when the same evaluation was performed after the 30 day period, slightly reduced  $\Delta E_{ab}^*$  values were recorded, specifically,  $5.4 \pm 0.4$ ,  $4.2 \pm 0.4$ ,  $3.7 \pm 0.2$ , for the 200, 100, 50 mg mL<sup>-1</sup> solutions, respectively (Figure 4a, right). It is worth noting that, at concentrations below 100 mg mL<sup>-1</sup>, all the values remained below the acceptable limit, within the error, for protective treatments ( $\Delta E_{ab}^* \leq 5$ ).<sup>49</sup> Accordingly, the  $\Delta E_{ab}^*$  values estimated for the mockups 1 day after application were lower for the less concentrated solutions (i.e.,  $3.1 \pm 0.4$ ,  $2.8 \pm 0.3$ , and  $2.0 \pm 0.2$  for the 10, 6, and 1 mg mL<sup>-1</sup> solutions, respectively). The same trend (decreasing  $\Delta E_{ab}^*$  values) was observed 30 days after

application. Overall, the CIELab results indicated that the POM-IL1 coating solutions, within the range of  $100 < [\text{mg mL}^{-1}] < 1$ , had a minimal visual impact on the color of mockups. The same general trend was observed for the mockups coated with POM-IL2 (Figure 4b,d).

In short, after a 30 day period of natural aging, the color variation derived by the application of the more concentrated POM-ILs solutions ( $200 \text{ mg mL}^{-1}$ ) are over the limit of the acceptable value ( $\Delta E_{ab}^* \leq 5$ ).<sup>49</sup> In the case of the  $100 \text{ mg mL}^{-1}$  solution of both POM-IL1 and POM-IL2, the resulting color variations were perceptible with the naked eye, although falling into the acceptable value,<sup>49</sup> within the error. Results obtained for the POM-IL1 coating solution of  $50 \text{ mg mL}^{-1}$  were on the established  $\Delta E_{ab}^*$  limit value ( $\Delta E_{ab}^* \leq 3$ ), within the error and the remaining solutions ( $10, 6,$  and  $1 \text{ mg mL}^{-1}$ ) of both POM-ILs caused color variations below this maximum perceptibility value.

Similar results were reported among the literature<sup>32,36,37</sup> while conducting studies using the same POM-ILs, although in different chalk and natural stones. As an example, Eyssautier-Chuine et al.<sup>36</sup> also observed a general darkening of the samples after applying the coatings (regardless of the type, POM-IL1 or POM-IL2), and similar trends of  $\Delta E_{ab}^*$  were determined for coatings with a concentration of  $100 \text{ mg mL}^{-1}$ .

$\Delta E_{ab}^*$  was also estimated for pre-aged mockups upon coating ( $R_{1b\_t_1\_x}$ ). The results obtained did not show considerable differences regardless of the aging period ( $t_1, t_2$ ). Therefore, only the results obtained for the first aging period ( $t_1$ ) will be discussed here. Still, the results considering the  $t_2$  aging period are available in Table S11 and Figure S5. It is worth noting that the  $R_{1b\_t_1}$  mockups underwent a color change due to the artificial aging procedure compared to the unaged mockups ( $R_{1b\_t_0}$ ). This aspect was considered when assessing the impact of the POM-IL coatings on the final color of the mockups.

When comparing the results obtained with those previously discussed, consistent trends in the color alterations can be found. In other words, more prominent color alterations were associated with coating solutions with higher concentrations (Figure 4c,d). However, lower overall  $\Delta E_{ab}^*$  values were estimated in this case, and both POM-IL1 and POM-IL2 coatings yielded results within the acceptable range. This can be attributed mainly to the yellowish hue of the mockups resulting from aging. Furthermore, the measurements performed on the mockups after the 30 day-period revealed interesting observations. Except for mockups coated with  $200 \text{ mg mL}^{-1}$  POM-IL1 and POM-IL2, all other samples exhibited color variations falling within or below the perceptibility limit (within the error). Briefly, the aged mockups had a yellowish hue compared to the unaged ones, resulting in fewer color alterations upon coating application, considering the pronounced effect on the yellow range ( $\Delta b^* > 0$ ).

Considering the overall results, the mockups coated with the  $200 \text{ mg mL}^{-1}$  POM-IL solution were excluded from further analyses because, at this concentration, color variations were above or close to the acceptable established limits for conservation treatment.<sup>49</sup>

Regarding the surface pH, the overall results showed that no considerable pH alterations occurred after applying the coatings regardless of the concentration that was used. For example,  $R_{1b\_t_0\_x}$  ( $x = \text{POM-IL1}$  or  $\text{POM-IL2}$ ) showed maximum pH values of  $3.2 \pm 0.0$  and  $3.1 \pm 0.1$ , respectively, which closely matched the pH values of the corresponding

uncoated ( $R_{1b\_t_0}$ ,  $\text{pH} = 4.0 \pm 0.0$ ). Similarly, pre-aged mockups ( $R_{1b\_t_1\_1}$  and  $R_{1b\_t_1\_2}$ ) exhibited pH values of  $3.0 \pm 0.0$ , also close to the pH value of the corresponding uncoated ( $R_{1b\_t_1}$  with a  $\text{pH} = 3.1 \pm 0.1$ ), within the error. Similar results were obtained for  $R_2$  mockups.

Keggin-type POMs have been recognized for being acid-stable and providing acid resistance in the artifacts where they are employed.<sup>32,50</sup> Thus, acidity fluctuations were not expected. Unfortunately, previous studies lacked pH evaluations. No direct comparison can then be made with the available literature. In short, it can be concluded that the coatings did not alter the pH of the mockups over the 30 day naturally aging period.

**Surface Morphology of the Mockups and POM-IL Penetration within Cellulose Structure.** Figure 5 shows

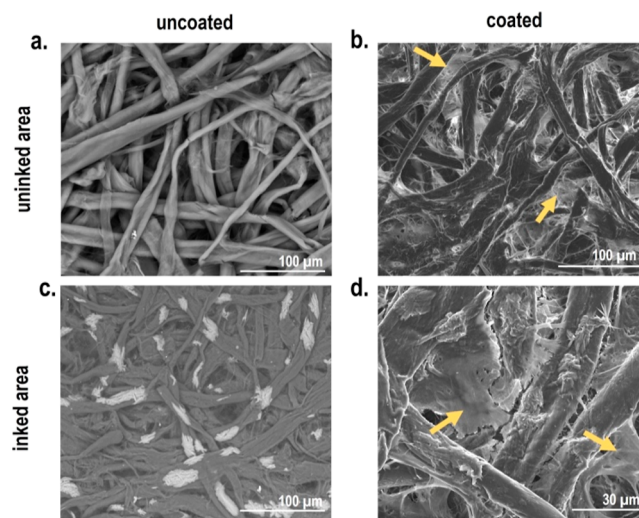


**Figure 5.** (a,c) SEM micrographs of uninked and inked areas of the  $R_{1b\_t_1}$  mockup prior to the coating application; (b,d) their corresponding coated areas. Yellow arrows highlight the presence of POM-IL1 coating between the voids of the cellulose fibers.

SEM micrographs of  $R_{1b\_t_1}$  mockups before and after the coating with POM-IL1 ( $100 \text{ mg mL}^{-1}$ ). Considering the coated mockups (Figure 5b,d), SEM observations revealed a nonuniform film-like formation on the cellulosic support surface. It was particularly evident between the voids of the cellulose fibers, resembling a spider web. Therefore, one can hypothesize that the coating might have enhanced the stability of cellulose fibers by filling the space between the voids, thus strengthening the cellulose structure. With this in mind, we posit that the coating could improve the mechanical properties, which will be discussed further below. Importantly, no changes in the morphology of the cellulose fibers were observed after the coating application. Since this is the first time POM-IL coatings have been used on IGI-containing cellulosic supports, no comparisons could be made among similar materials. Nonetheless, while applying POM-IL coatings on stone materials, Misra et al.<sup>32</sup> reported the formation of a surface layer with a homogeneous distribution. We attributed the differences between the distribution of the coatings to the physical characteristics of the supports.

It is worth noting that in the  $R_{1b\_t_1\_1}$  mockup, the coating was observed to trap agglomerates of particles found on the surface and within the cellulose fibers. This occurrence was especially evidenced in the SEM micrograph depicted in

**Supporting Information** Figure S6. As discussed in the mockups characterization section (see **Supporting Information** section 5), these particles consist of Fe(II) oxalate crystals associated with a degradation compound formed over aging in the mockups. We hypothesized that this trapping phenomenon can potentially minimize the mobility of free Fe(II) ions, thereby mitigating the ongoing formation of Fe(II) oxalates and IGI corrosion. Based on similar reasoning, the coating might also limit the interaction of the uppermost layer of the cellulosic support with the environment (e.g., atmospheric oxygen and moisture), acting as a barrier, thus providing additional protection against the extent of ongoing oxidation processes.

Given that the Fe(II) penetration through cellulose fibers is a primary concern in IGI-containing documents, POM-ILs must also penetrate the cellulose structure to achieve an optimum effect as an effective conservation treatment. EDS line measurements and point analyses were conducted to assess the spatial distribution of Fe from the IGI and W from the POM-IL to better understand the depth of penetration of the POM-ILs. Therefore, cross sections of the unaged coated mockups (R<sub>1</sub>b\_t<sub>0</sub>\_x) with the 100, 50, and 6 mg mL<sup>-1</sup> POM-ILs solutions were prepared. For mockups coated with concentrated solutions (100 and 50 mg mL<sup>-1</sup>), W was detected on the surface and the inner areas of the cellulosic support, in addition to Fe from the IGI (**Figure 6a**). The

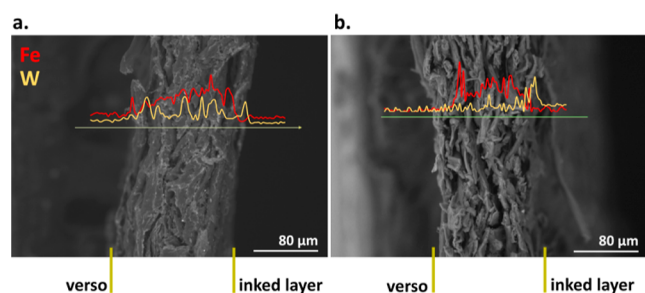


**Figure 6.** (a) SEM/EDS line scan profiles of Fe K (red line) and W K (yellow line) measured on a cross-section of the R<sub>1</sub>b\_t<sub>0</sub>\_1 mockup coated with POM-IL1 at: (a) 100; (b) 6 mg mL<sup>-1</sup>.

amount of W on the surface ranged from ~1–12 wt %, while EDS point analysis of the inner areas revealed 1 to 3 wt % W, compared to 4–16 wt % Fe. In contrast, mockups coated with the most dilute POM-IL solution, 6 mg mL<sup>-1</sup>, exhibited very low amounts of W (<1 wt %) in the inner areas (**Figure 6b**), indicating poorer penetration of the POM-IL into the inner network of cellulose fibers.

**FT-IR Analysis.** The FT-IR spectra of R<sub>1</sub>b\_t<sub>0</sub> before and after the coating application, band assignment and respective interpretation are detailed in **Figure S7** and **Table S12**. The uncoated mockups exhibited the typical bands of the cellulosic support, which were previously presented (see **Supporting Information** 5). Furthermore, the IGI bands were also identified at ca. 1640 cm<sup>-1</sup> [ $\delta$ (O–H) adsorbed water], 1459 cm<sup>-1</sup> [ $\nu_{as}$ (S–O)], 1320 cm<sup>-1</sup> [ $\nu_s$ (C–O)], 1044 cm<sup>-1</sup> [ $\nu_s$ (C–O)], 951 cm<sup>-1</sup> [ $\nu_s$ (S–O)] and 658 cm<sup>-1</sup> [ $\nu_{as}$ (Fe–O)].

Only the more significant alterations in the FT-IR features that evolved with the coating application will be discussed here. Nevertheless, the characteristic bands of the POM-IL were not clearly evidenced due to the overlap with the coating and cellulose bands, making interpretation challenging.

The features at ca. 2921 [ $\nu_s$ (CH<sub>2</sub>)] and 2852 cm<sup>-1</sup> [ $\nu_{as}$ (CH<sub>2</sub>)] were associated with the organic cation (tetraheptylammonium (THepA)), which is aligned with the spectral features of POM-IL.<sup>32</sup> In addition, the IR spectrum of R<sub>1</sub>b\_t<sub>0</sub>\_1 exhibited small bands at ca. 1053 cm<sup>-1</sup> [ $\nu$ (Si–O–Si)], 964 cm<sup>-1</sup> [ $\nu$ (W–O<sub>c</sub>)], 908 cm<sup>-1</sup> (W–O<sub>b</sub>–W) and 801 cm<sup>-1</sup> [ $\nu_{as}$ (W–O<sub>a</sub>–W)] associated with the POM framework.<sup>32,51</sup> In the R<sub>1</sub>b\_t<sub>0</sub>\_1, the bands at ca. 908 and 801 cm<sup>-1</sup> were slightly shifted to higher wavenumbers regarding the pure POM features (see **Figure S2**). Furthermore, the increased intensity of the bands at ca. 663 suggests the presence of Fe–O–W.<sup>52</sup>

Additionally, special attention was given to the bands associated with the cellulose structure, specifically, 1426 cm<sup>-1</sup> [ $\delta$ (CH<sub>2</sub>) in crystalline region] and 898 cm<sup>-1</sup> [ $\nu$ (C–O–C) assigned to the amorphous region].<sup>53,54</sup> As explained in the mockups characterization, variation in the shape and intensity of these features has been used to study alterations in the crystallinity of cellulose.<sup>53,54</sup> As no considerable changes were observed between the coated and uncoated sample, one can suggest that POM-IL coating did not promote considerable adverse effects on the cellulose structure.

**Physical Properties Testing.** Although the primary goal of the POM-IL treatment was not consolidation, structural and mechanical tests were performed to evaluate its mechanical effects on the mockups (**Table S6**). The physical tests were conducted only on mockups subjected to the t<sub>2</sub> aging period (R<sub>1</sub> ink), t<sub>1</sub> aging period (R<sub>2</sub> ink) and corresponding coated mockups. Due to the physical fragility of R<sub>2</sub>\_a\_t<sub>1</sub> mockups, we decided to stop the aging procedure at this point. Additionally, only the mockups coated with POM-IL1 (100 mg mL<sup>-1</sup>) were tested due to the large number of samples needed to ensure statistically significant values. The results obtained regarding the structural properties such as grammage, thickness, apparent density, and the air permeability Bendtsen method are shown in **Table S13**.

The grammage values ranged from 84 ± 1 to 89 ± 2 g m<sup>-2</sup>, with the lowest values corresponding to the pre-aged mockups, regardless of the presence of coatings. These results highlight the aging procedure as the key factor for the variations among the grammage values. Similar observations were found for the remaining parameters, indicating that POM-IL coatings did not interfere with the structural properties of the mockups. Following, tensile strength and zero-span tests were conducted. The tensile strength test informs about the maximum stress a material can bear before breaking<sup>55</sup>, and the dry zero-span parameter validates the damage to the fibers, considering factors like the thickness of the fiber cell wall and the fiber diameter.<sup>56</sup> An overall prominent decline in the tensile index (ca. 95%) was observed for the pre-aged R<sub>1</sub> and R<sub>2</sub> mockups compared to the unaged mockups (**Figure S8a**). As no considerable differences within the error were observed between the uncoated and coated mockups, the decrease in the tensile index was primarily attributed to the aging procedure, further potentiated by the impact of IGI. Additionally, the zero-span study (**Figure S8b**) showed decreasing values for R<sub>1</sub> and R<sub>2</sub> pre-aged mockups compared to their corresponding unaged ones. This result strongly implies that the presence of IGI compromised the fiber strength. The coated mockups exhibited similar values within the error, indicating no discernible effect attributed to the presence of POM-ILs on the fiber damage. Indeed, the presence of the POM-IL1 coating did not limit the decline of the physical



properties of the mockups. Consequently, if a consolidating effect were to be achieved, these results suggested the need to explore whether using a coating with a higher concentration can yield more successful results. It is crucial to keep in mind that the maximum value to consider should be below 200 mg mL<sup>-1</sup>, as previously discussed. Importantly, these results strongly suggest that POM-ILs do not compromise the integrity of the cellulose structure in IGI-containing documents. This insight is of utmost importance, given that ILs have been explored and documented in cellulose dissolution-oriented research.<sup>57,58</sup> As evidenced, factors such as the concentration play a decisive role in determining the goals to be achieved.

## ■ PHASE II—EVALUATION OF THE PERMANENCE OF POM-IL COATINGS, THEIR IMPACT ON THE MOCKUPS, AND EFFECTIVENESS IN LIMITING IGI CORROSION THROUGH ARTIFICIAL AGING

This section presents the evaluation of the long-term stability of the POM-IL coatings and their impact on the mockups over aging. Based on the results from phase I, only the mockups coated with POM-IL coatings of 100 mg mL<sup>-1</sup> were studied.

Overall, limited color variations were observed for the R<sub>1</sub>b, R<sub>1</sub>w, R<sub>2</sub>b, and R<sub>2</sub>w mockups, regardless of the coating (POM-IL1 or POM-IL2). Therefore, only the results of R<sub>1</sub>b mockups are discussed here for simplicity. The complete set of results for the remaining mockups (R<sub>1</sub>w, R<sub>2</sub>b, and R<sub>2</sub>w) are available in Supporting Information (Tables S14–S17). It is important to note that the mockups undergo color changes once subjected to artificial aging, which was discussed in the previous work (see Supporting Information 5). Thus, to evaluate the impact of the coatings over aging, color measurements were conducted on samples from phase II (both uncoated and coated) subjected to corresponding aging periods.

No considerable color alterations occurred in the coated R<sub>1</sub>b mockups regardless of the aging periods and the coating (POM-IL1 or POM-IL2) (Figure S1). After artificial aging ( $t_1$  and  $t_2$ ), values of  $\sim 2$ – $4$  for  $\Delta E_{ab}^*$  were estimated for R<sub>1</sub>b coated with either POM-IL1 or POM-IL2. Regarding the mockups subject to a reaging procedure, values of  $\sim 2$  for  $\Delta E_{ab}^*$  were determined for both coatings. Therefore, the global color alteration remained consistently close to or below the perceptibility limit ( $\Delta E_{ab}^* \leq 3$ ), pointing out that the resulting color variations were imperceptible to the naked eye.<sup>49</sup>

The coated mockups became slightly darker ( $\Delta L^* < 0$ ) in comparison to the uncoated ones, with the aged mockups ( $t_2$ ) coated with POM-IL2 (Figure S9) showing the highest decrease in the  $\Delta L^*$  (i.e.,  $2.4 \pm 0.6$ ), within the error. Nevertheless, regardless of the coating, no trend was identified for the aged or the reaged mockups. The  $\Delta a^*$  and  $\Delta b^*$  presented only minute alterations over aging. As per the reaged mockups, R<sub>1</sub>b\_a\_t<sub>4</sub> exhibited a lower yellowish contribution than R<sub>1</sub>b\_a\_t<sub>3</sub>, similar to what was observed for the R<sub>1</sub> mockups coated with POM-IL2 (Figure S9). In brief, POM-IL coatings had minimal impact on mockup colors over aging. Next, SEM/EDS analysis confirmed that the POM-IL coating did not undergo any undesired morphological changes (e.g., crystallization, precipitation, agglomeration) during the aging or reaging. Importantly, the presence of the coating also did not lead to alterations in the cellulosic support during aging.

The hydrophobic properties of the POM-IL likely prevented unwanted modifications from occurring. EDS analysis was used to assess the wt % of W on the R<sub>1</sub>b\_a\_t<sub>1</sub>, which ranged from 0.75 to 3.12%. Although these values are lower than those previously discussed for phase I, they still provide clear evidence of the POM-ILs on the mockups, thereby confirming their stability over aging.

The coating stability as a function of aging, as well as alterations to the mockups structure, were assessed by FT-IR analysis. The IR spectra of the unaged (R<sub>1</sub>b\_t<sub>0</sub>) and aged (R<sub>1</sub>b\_a\_t<sub>1</sub>) uncoated mockups, together with the corresponding mockups coated with POM-IL1 (R<sub>1</sub>b\_t<sub>0</sub>\_1 and R<sub>1</sub>b\_a\_t<sub>1</sub>\_1) are shown in Figure 7. Typical IR features of

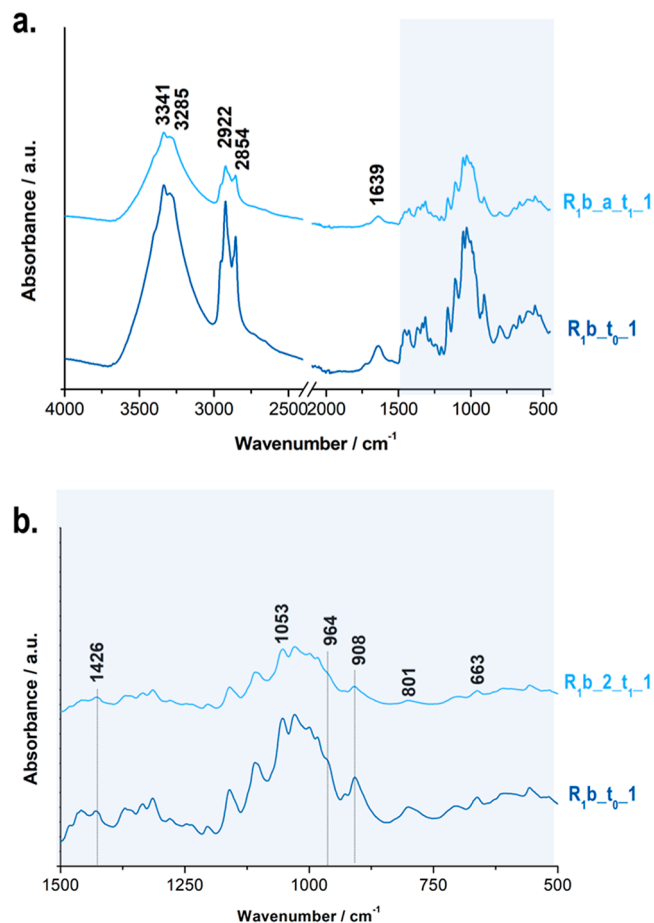


**Figure 7.** (a) FT-IR full region spectra of the unaged (R<sub>1</sub>b\_t<sub>0</sub>\_1) and aged (R<sub>1</sub>b\_a\_t<sub>1</sub>\_1) coated mockups; (b) zooming of the region of interest (1500–500 cm<sup>-1</sup>) where the cellulose crystalline-related bands (1426 and 908 cm<sup>-1</sup>) and the POM-ILs bands (1053, 964, 908, 801, 663 cm<sup>-1</sup>) were labeled. The spectra are vertically offset for clarity, and color grading is used for better visualization.

cellulose and IGI were identified and previously discussed. Unfortunately, the IR features related to the POM-ILs which evolve in the region between 500 and 1100 cm<sup>-1</sup>,<sup>32,51</sup> were considerably overlapped by those of the cellulosic support, making the FT-IR interpretation challenging. Nevertheless, the characteristic bands of the POM-IL were identified, which confirms the permanence of the coating on the mockups over aging.

A slight drop in the intensity of the bands at 3341 and 3285 cm<sup>-1</sup>  $\nu_s$ (OH) of the aged coated mockups (R<sub>1</sub>b\_a\_t<sub>1</sub>\_1) was

observed when compared to that of the unaged coated ones ( $R_{1b\_t_0\_1}$ ). A similar behavior was found and reported for the uncoated mockups (see phase I, FT-IR Analysis section). As documented in the literature, these alterations in the OH-features are likely due with the cleavage of intra- and intermolecular H-bonds, leading to structural changes in the cellulosic support.<sup>54,59,60</sup> This was primarily attributed to the aging procedure, as discussed in our previous work.<sup>38</sup>

In addition, the bands at 2922 and 2852  $\text{cm}^{-1}$  corresponding to  $-\text{CH}_2$  vibrations, to which the presence of ionic liquids from the POM-ILs strongly contributed, were found to decreased in intensity in the aged, coated mockups regarding the corresponding unaged. This implies that the aging procedure partially affected the stability of the coatings.

Special attention was given to the band at *ca.* 1639  $\text{cm}^{-1}$ , associated with the adsorbed water molecules [ $\delta(\text{OH})$ ], though also linked to the carbonyl group arising from paper degradation.<sup>61</sup> In our previous work,<sup>38</sup> the FT-IR study conducted on the mockups subjected to artificial aging showed that this feature tends to increase during aging due to the ongoing oxidation mechanism of the C-OH groups in the glucopyranose rings. Here, in the aged, coated mockups ( $R_{1b\_a\_t_1\_1}$ ), this feature showed no considerable variations. Indeed, this behavior suggest that the POM-IL coating may limit the extent of cellulose oxidation. However, care must be taken when interpreting this result because the presence of a small shoulder at *ca.* 1670  $\text{cm}^{-1}$ , indicates the occurrence of degradation.<sup>38,61</sup> Notably, both features were also observed in the unaged coated mockups, indicating that the coating did not have a negative effect on the support. As explained in the FT-IR results of phase I, alterations in the cellulose crystallinity can be investigated by the behavior of the 898  $\text{cm}^{-1}$  [ $\nu(\text{C}-\text{O}-\text{C})$ ] and 1426  $\text{cm}^{-1}$  [ $\delta(\text{CH}_2)$ ] features.<sup>53,54</sup> Both features were slightly broader and decreased in intensity over aging, confirming the occurrence of changes in the cellulose structure. Nevertheless, as a similar behavior was observed on the uncoated mockups, those alterations were primarily attributed to the IGI impact on the cellulosic support, further prompted by the aging procedure. Indeed, this result provides unequivocal support that the concentration of the POM-ILs in use does not adversely affect the cellulose structure. Finally, the band *ca.* 663  $\text{cm}^{-1}$  (assigned to Fe-O-W), appeared slightly uppershifted and with higher intensity when compared to the corresponding uncoated (660  $\text{cm}^{-1}$ ), suggesting the interaction of the POM-IL coating with the iron from the IGI.

Overall, IR data confirmed the permanence of the coatings on the mockups even after artificial aging and established that the POM-IL coatings had no apparent adverse effect on the structure of the cellulosic support over the tested period.

## CONCLUSIONS

This investigation was based on a two-fold approach: first, a proof-of-concept was developed to assess the ability of POM-ILs to chelate free Fe(II); subsequently, dilute POM-IL solutions were brush-coated on IGI mockups to evaluate their impact and optimize the coating concentration (phase I). Finally, their permanence of the POM-IL coatings and their capacity to counteract IGI-corrosion was explored through artificial aging of the samples (phase II) and subsequent analysis using a combination of colorimetry, SEM/EDS, and FT-IR. Overall, POM-ILs emerge as candidates for addressing two unresolved challenges in IGI conservation: countering the presence of free Fe(II) and meeting the demand of

conservation treatments that ensure the preservation of ancient IGI documents without compromising their structural integrity and historical value.

In the first phase (phase I), the capacity of the POMs to bind Fe(II) ions from IGI solutions was verified using UV-vis spectroscopy, demonstrating the capacity of the POMs to coordinate free Fe(II) ions which catalyze IGI-corrosion processes. The crystallization of the dimeric Fe(III)-substituted polyoxotungstate  $[(\text{SiW}_{11}\text{O}_{39}\text{Fe})_2\text{O}]^{12-}$  supported this property. The deployment of POM-IL as protective coatings ( $\leq 100 \text{ mg mL}^{-1}$ ) on the mockups resulted in color alterations close to or below the acceptable value ( $\Delta E_{ab}^* \leq 5$ ), meeting the requirements of conservation treatments. Additionally, SEM/EDS was used to study POM-IL penetration within the cellulose structure in coated mockup cross sections. The results showed successful penetration when the POM-IL concentration ranged from 50 to 100  $\text{mg mL}^{-1}$ . Effective penetration is essential, since free Fe(II) ions in the inner layers of cellulose structures are key drivers of IGI-induced degradation.

According to phase II results, POM-ILs deployed as protective conservation coatings on model IGI-containing papers (mockups) and artificially aged confirmed their compatibility with the written and support material and attested that artificial aging did not affect the permanence of the coatings. Notably, extensive FT-IR studies showed no considerable alterations in the carbonyl group arising from cellulose degradation in the coated mockups compared to uncoated mockups, irrespective of the aging periods. These results strongly indicate that POM-ILs counteract IGI-corrosion. Nevertheless, it is crucial to acknowledge the inherent risks associated with the permanent and irreversible use of POM-ILs. The long-term implications of introducing POM-ILs to written cultural heritage must be carefully considered. Therefore, further studies, including more comprehensive artificial aging, are essential to better understand their behavior and the potential issues arising from their interaction with IGI-containing samples over time.

Finally, SEM revealed a spider web-like film forming in the space between the voids of the cellulose fibers, providing a first indication that the coatings could also improve the stability of the cellulose structure. Besides, it is also likely that the POM-IL interface acts as a protective barrier to reduce the interaction between the cellulosic support and environmental factors: reducing moisture ingress as well as the deposition of other airborne pollutants and microbes, which can also accelerate existing corrosion mechanisms. However, these aspects remain to be confirmed. As standardized protocols for evaluating IGI corrosion mitigation on paper-based documents are lacking, assessing and comparing different treatments becomes challenging. Therefore, future work aimed at understanding the potential of POM-ILs for IGI conservation treatments must investigate their effectiveness through combined surface and bulk analyses and address the long-term performance of POM-ILs on IGI-containing historical samples in library and archival contexts is imperative.

## ASSOCIATED CONTENT

### Supporting Information

The Supporting Information is available free of charge at <https://pubs.acs.org/doi/10.1021/acsomega.4c04925>.

(i) Synthesis and characterization; (ii) inks reproduction; (iii) mockups preparation, characterization, and artificial aging procedures; (iv) POM-IL coatings preparation, application, and reaging procedure; (v) single crystal X-ray data and FT-IR spectrum of  $[(\text{SiW}_{11}\text{O}_{39}\text{Fe})_2\text{O}]_{\text{K}_{12}}\cdot 28\text{H}_2\text{O}$ ; (vi) characterization of the impact of the POM-IL coatings on the mockups using colorimetry, SEM/EDS, FT-IR (PDF)

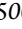
### Accession Codes

CCDC-2324283 contains the supplementary crystallographic data for this paper. These data can be obtained free of charge from the Cambridge Crystallographic Data Centre via [www.ccdc.cam.ac.uk/structures/](http://www.ccdc.cam.ac.uk/structures/).

## AUTHOR INFORMATION

### Corresponding Authors

**Ana Claro** – CHAM-Centre for the Humanities, College of Social and Human Sciences, NOVA University of Lisbon, Lisboa 1099-085, Portugal; Email: [aclaro@fch.unl.pt](mailto:aclaro@fch.unl.pt)

**Scott G. Mitchell** – Instituto de Nanociencia y Materiales de Aragón (INMA), CSIC-Universidad de Zaragoza, Zaragoza 50009, Spain;  [orcid.org/0000-0003-4848-414X](https://orcid.org/0000-0003-4848-414X); Email: [scott.mitchell@csic.es](mailto:scott.mitchell@csic.es)

### Authors

**Margarida Nunes** – HERCULES Laboratory/IN2PAST, Associate Laboratory for Research and Innovation in Heritage, Arts, Sustainability and Territory, University of Évora, Évora 7004-516, Portugal

**Pilar García-Orduña** – Instituto de Síntesis Química y Catálisis Homogénea (ISQCH), CSIC-Universidad de Zaragoza, Zaragoza 50009, Spain

**Elena Atrián-Blasco** – Instituto de Nanociencia y Materiales de Aragón (INMA), CSIC-Universidad de Zaragoza, Zaragoza 50009, Spain

**Joana Costa Vieira** – FibEnTech-UBI, Fiber Materials and Environmental Technologies, University of Beira Interior, Covilhã 6201-001, Portugal

**Ana Paula Costa** – FibEnTech-UBI, Fiber Materials and Environmental Technologies, University of Beira Interior, Covilhã 6201-001, Portugal

**Maria Emília Cabral Amaral** – FibEnTech-UBI, Fiber Materials and Environmental Technologies, University of Beira Interior, Covilhã 6201-001, Portugal

**Teresa Ferreira** – HERCULES Laboratory/IN2PAST, Associate Laboratory for Research and Innovation in Heritage, Arts, Sustainability and Territory and Chemistry and Biochemistry Department at the Sciences and Technology School, University of Évora, Évora 7004-516, Portugal

Complete contact information is available at:

<https://pubs.acs.org/10.1021/acsomega.4c04925>

### Author Contributions

A.C., S.G.M., M.N.—conceptualization; M.N. and S.G.M.—methodology; M.N. and E.A.-B.—synthesis; M.N.—formal analysis and data interpretation; P.G.-O.—single-crystal X-ray diffraction analysis and data interpretation; J.C.V., A.P.C., M.E.A.C., M.N.—physical tests and data interpretation; S.G.M.—supervision; M.N., S.G.M.— Writing-original draft; All authors—review and editing.

### Funding

This work was carried out within the framework of the project IRONiC—Iron Gall Ink Challenges (IronIC)—History and Conservation of a Disappearing Cultural Heritage (PTDC/ART-HIS/32327/2017) funded by FCT. The authors are grateful for the FCT support through the PhD grant (SFRH/BD/147528/2019) and the additional grant due to the COVID-19 pandemic crisis (COVID/BD/153467/2023). This work was funded through the grant PID2022–141276OB-I00 and CEX2023–001286-S funded by MCIN/AEI/10.13039/501100011033 (Ministerio de Ciencia e Innovación/Agencia Estatal de Investigación, Spain). This study was supported by MCIN with funding from the European Union NextGenerationEU (PRTR-C17.I1) promoted by the Government of Aragón. There was the collaboration of the research unit HERCULES Laboratory/IN2PAST (10.54499/UIDP/04449/2020, 10.54499/UIDB/04449/2020 & LA/P/0132/2020) and the Fiber Materials and Environmental Technologies (FibEnTech-UBI), on the extent of the project reference UIDB/00195/2020, funded by national funds through the IP/MCTES (PIDDAC).

### Notes

The authors declare no competing financial interest.

## ACKNOWLEDGMENTS

The authors acknowledge the Laboratorio de Microscopias Avanzadas (LMA) at the University of Zaragoza for offering access to their instruments and expertise, and Prof. Fernando J. Lahoz for fruitful discussions about single crystal structure.

## REFERENCES

- (1) Carvalho, D. N. *Forty Centuries Of Ink*; The Banks Law Publishing Co., 1904.
- (2) Rabin, I. Material Studies of Historic Inks: Transition from Carbon to Iron-Gall Inks. *Traces of ink - Experiences of Philology and Replication*; Raggeti, L., Ed.; Brill: Leiden, 2021.
- (3) Kolar, J.; Strlic, M. Ageing and Stabilisation of Paper Containing Iron Gall Ink. *Prototype InkCor treatments: Evaluation of effectiveness*; Kolar, J., Strlic, M., Eds.; National and University Library, 2006.
- (4) Nunes, M.; Olival, F.; Mitchell, S. G.; Claro, A.; Ferreira, T. A Holistic Approach to Understanding the Iron-Gall Inks in the Historical Documents of the Portuguese Inquisition (1570–1790). *Micron* **2023**, *165* (December 2022), 103396.
- (5) Montani, I.; Sapin, E.; Pahud, A.; Margot, P. Enhancement of Writings on a Damaged Medieval Manuscript Using Ultraviolet Imaging. *J. Cult. Herit.* **2012**, *13* (2), 226–228.
- (6) Liu, Y.; Kralj Cigić, I.; Strlič, M. Kinetics of Accelerated Degradation of Historic Iron Gall Ink-Containing Paper. *Polym. Degrad. Stab.* **2017**, *142* (1), 255–262.
- (7) Kolar, J.; Strlič, M.; Budnar, M.; Malešič, J.; Šelih, V. S.; Simčič, J. Stabilisation of Corrosive Iron Gall Inks. *Acta Chim. Slov.* **2003**, *50* (4), 763–770.
- (8) Cultural Heritage Agency of the Netherlands, R. iron gall ink website. <https://irongallink.org/> (accessed on Feb 13, 2011).
- (9) Nunes, M.; Claro, A.; Ferreira, T. Nada Há de oculto que não venha a revelar-se. O contributo do estudo material para a desconstrução do códice 99 do Fundo Da Manizola. *Orthographia, Arithmetica, Siencias - Três tratados do P.e António Pessoa (c. 1648 S.J.)*; Claro, A., Ferreira, T., Reis Miranda, T., Nunes, M., Eds.; Coord.; Scribe: Lisboa, 2023; pp 19–44.
- (10) Miguel, C.; Claro, A.; Gonçalves, A. P.; Muralha, V. S. F.; Melo, M. J. A Study on Red Lead Degradation in a Medieval Manuscript Lorrão Apocalypse (1189). *J. Raman Spectrosc.* **2009**, *40* (12), 1966–1973.
- (11) Kolar, J. INKCOR - stabilisation of iron gall ink containing paper. InkCor project. <https://cordis.europa.eu/article/id/85417->

protecting-historical-documents-from-corrosive-ink (accessed on Mar 01, 2012).

(12) DGRARQ-TT. Apocalipse do Lorvão. <https://digitarq.arquivos.pt/details?id=4381091> (accessed on Mar 04, 2023).

(13) Aceto, M.; Agostino, A.; Fenoglio, G.; Capra, V.; Demaria, E.; Cancian, P. Characterisation of the Different Hands in the Composition of a 14th Century Breviary by Means of Portable XRF Analysis and Complementary Techniques. *X-Ray Spectrom.* **2017**, *46* (4), 259–270.

(14) Aceto, M.; Calà, E. Analytical evidences of the use of iron-gall ink as a pigment on miniature paintings. *Spectrochim. Acta, Part A* **2017**, *187*, 1–8.

(15) Kroustallis, S. La Tinta Negra Ferrotánica: A Propósito de Las Fuentes. In *V Congreso Nacional de Historia del Papel. Actas; Ajuntament de Sarrià de Ter*, 2003; pp 238–259.

(16) Neevel, J. The Development of a New Conservation Treatment for Ink Corrosion, Based on the Natural Anti-Oxidant Phytate. *8th IADA Congr.; IADA*, 1995; pp 93–100.

(17) Rouchon-Quillet, V.; Remazeilles, C.; Bernard, J.; Wattiaux, A.; Fournes, L. The Impact of Gallic Acid on Iron Gall Ink Corrosion. *Appl. Phys. A: Mater. Sci. Process.* **2004**, *79* (2), 389–392.

(18) Liu, Y.; Kralj-cigić, I.; Strlič, M. Kinetics of Accelerated Degradation of Historical Iron Gall-Containing Paper. *Polym. Degrad. Stab.* **2017**, *142*, 255.

(19) Rouchon, V.; Bernard, S. Mapping Iron Gall Ink Penetration within Paper Fibres Using Scanning Transmission X-ray Microscopy. *J. Anal. At. Spectrom.* **2015**, *30* (3), 635–641.

(20) Rouchon, V.; Duranton, M.; Cédric, B.; Pellizzi, E.; Lavédrine, B.; Janssens, K.; de Nolf, W.; Nuyts, G.; Vanmeert, F.; Hellemans, K. Room-Temperature Study of Iron Gall Ink Impregnated Paper Degradation under Various Oxygen and Humidity Conditions: Time-Dependent Monitoring by Viscosity and X-ray Absorption Near-Edge Spectrometry Measurements. *Anal. Chem.* **2011**, *83* (7), 2589–2597.

(21) Potthast, A.; Rosenau, T.; Kosma, P. Analysis of Oxidized Functionalities in Cellulose. *Adv. Polym. Sci.* **2006**, *205* (1), 1–48.

(22) Völkel, L.; Prohaska, T.; Potthast, A. Combining Phytate Treatment and Nanocellulose Stabilization for Mitigating Iron Gall Ink Damage in Historic Papers. *Herit. Sci.* **2020**, *8* (1), 1–15.

(23) Neevel, J. G. Phytate: A Potential Conservation Agent for the Treatment of Ink Corrosion Caused by Iron Gall Inks. *Restaurator* **1995**, *16* (3), 143–160.

(24) Kolar, J.; Možir, A.; Strlič, M.; de Bruin, G.; Pihlar, B.; Steemers, T. Stabilisation of Iron Gall Ink: Aqueous Treatment with Magnesium Phytate. *e-Preserv. Sci.* **2007**, *4*, 19–24.

(25) Gimat, A.; Michelin, A.; Massiani, P.; Rouchon, V. Beneficial Effect of Gelatin on Iron Gall Ink Corrosion. *Herit. Sci.* **2021**, *9* (1), 125–213.

(26) Malešič, J.; Kolar, J.; Rtd, M.; Malešič, J.; Kolar, J.; Strlič, M.; Polanc, S. Use of Halides for Stabilisation of Iron-Gall Ink Containing Paper-The Pronounced Effect of Cation. *e-Preserv. Sci.* **2005**, *2*, 13.

(27) Botti, L.; Mantovani, O.; Ruggiero, D. Calcium Phytate in the Treatment of Corrosion Caused by Iron Gall Inks: Effects on Paper. *Restaurator* **2005**, *26* (1), 44–62.

(28) Huhsmann, E.; Hähner, U. Work Standard for the Treatment of 18th- and 19th-Century Iron Gall Ink Documents with Calcium Phytate and Calcium Hydrogen Carbonate. *Restaurator* **2008**, *29* (4), 274–319.

(29) Giorgi, R.; Baglioni, P.; Sistach, M. C.; Garcia, J. F.; Poggi, G.; Marin, E. Calcium Hydroxide Nanoparticles in Hydroalcoholic Gelatin Solutions (GeolNan) for the Deacidification and Strengthening of Papers Containing Iron Gall Ink. *J. Cult. Herit.* **2016**, *18*, 250–257.

(30) Kolar, J.; Strlič, M. *Ageing and Stabilisation of Paper*; National and University Library, 2005.

(31) Rouchon, V.; Duranton, M.; Belhadj, O.; Bastier-Deroches, M.; Duplat, V.; Walbert, C.; Hansen, B.; Hansen, B. V. The Use of Halide Charged Interleaves for Treatment of Iron Gall Ink Damaged Papers. *Polym. Degrad. Stab.* **2013**, *98*, 1339–1347.

(32) Misra, A.; Franco Castillo, I.; Müller, D. P.; González, C.; Eyssautier-Chuine, S.; Ziegler, A.; de la Fuente, J. M.; Mitchell, S. G.; Streb, C. Polyoxometalate-Ionic Liquids (POM-ILs) as Anticorrosion and Antibacterial Coatings for Natural Stones. *Angew. Chem., Int. Ed.* **2018**, *57* (45), 14926–14931.

(33) Mitchell, S. G.; De La Fuente, J. M. The Synergistic Behavior of Polyoxometalates and Metal Nanoparticles: From Synthetic Approaches to Functional Nanohybrid Materials. *J. Mater. Chem.* **2012**, *22* (35), 18091–18100.

(34) Rajkowska, K.; Koziróg, A.; Otlewska, A.; Piotrowska, M.; Atrián-Blasco, E.; Franco-Castillo, I.; Mitchell, S. G. Antifungal Activity of Polyoxometalate-Ionic Liquids on Historical Brick. *Molecules* **2020**, *25* (23), 5663.

(35) Franco Castillo, I.; Garcíaguillén, E.; M. De La Fuente, J.; Silva, F.; Mitchell, S. G. Preventing Fungal Growth on Heritage Paper with Antifungal and Cellulase Inhibiting Magnesium Oxide Nanoparticles. *J. Mater. Chem. B* **2019**, *7* (41), 6412–6419.

(36) Eyssautier-Chuine, S.; Franco-Castillo, I.; Misra, A.; Hubert, J.; Vaillant-Gaveau, N.; Streb, C.; Mitchell, S. G. Evaluating the Durability and Performance of Polyoxometalate-Ionic Liquid Coatings on Calcareous Stones: Preventing Biocolonisation in Outdoor Environments. *Sci. Total Environ.* **2023**, *884* (May), 163739.

(37) Franco-Castillo, I.; Misra, A.; Laratte, S.; Gommeaux, M.; Perarnau, R.; Vaillant-Gaveau, N.; Pierlot, C.; Streb, C.; Mitchell, S. G.; Eyssautier-Chuine, S. New Protective Coatings against Lampenflora Growing in the Pommery Champagne Cellar. *Int. Biodeterior. Biodegrad.* **2022**, *173* (June), 105459.

(38) Nunes, M.; Costa Vieira, J.; Costa, A. P.; Cabral, M. E.; Vieira, B. J. C.; Waerenorgh, J. C.; Nogueira, H. I. S.; Mitchell, S. G.; Claro, A.; Ferreira, T. *Advancing understanding of iron gall inks - an integrated multi-analytical approach for characterising ink reproductions*; Heliyon, 2024.

(39) ISO 5630–3:1996 Paper and Board-Accelerated Ageing-Part 3: Moist Heat Treatment at 80 Degrees C and 65% Relative Humidity; International Organization for Standardization: Geneva, Switzerland, 1996.

(40) Santos, F.; Brandão, P.; Félix, V.; Domingues, M. R.; Amaral, J.; Amaral, V.; Nogueira, H.; Cavaleiro, A. Organic-Inorganic Hybrid Materials Based on Iron(III)-Polyoxotungstates and 1-Butyl-3-Methylimidazolium Cations. *Dalton Trans.* **2012**, *41* (39), 12145.

(41) Junk, P. C.; McCool, B. J.; Moubaraki, B.; Murray, K. S.; Spiccia, L.; Cashion, J. D.; Steed, J. W. Utilization of Crown Ethers to Stabilize the Dinuclear  $\mu$ -Oxo Bridged Iron (III) Aqua Ion,  $[(\text{H}_2\text{O})\text{SFe}(\mu\text{-O})\text{Fe}(\text{OH}_2)_5]^{4+}$ . *J. Chem. Soc. Dalt. Trans.* **2002**, No. 6, 1024–1029.

(42) Kurtz, D. M. Oxo- and Hydroxo-Bridged Diiron Complexes: A Chemical Perspective on a Biological Unit. *Chem. Rev.* **1990**, *90* (4), 585–606.

(43) Sun, Z. G.; Liu, J. T.; Liu, J. F.; Li, J. Synthesis and Spectroscopic Characterization of Organophosphoryl Polyoxotungstates  $\alpha$ -A-[RP(O)]<sub>2</sub>PW<sub>9</sub>O<sub>34</sub><sup>5-</sup>. *Chem. Res. Chin. Univ.* **1999**, *16* (1), 90–92.

(44) Xue, Y.; Chen, J.; Shao, J.; Han, L.; Li, W.; Sui, C. Synthesis, catalytic activity and the structural transformation of dimeric mono-Fe(III)-substituted Keggin-type polyoxotungstates in the oxidation of cyclohexanol with H<sub>2</sub>O<sub>2</sub>. *Mol. Catal.* **2020**, *492* (May), 111010.

(45) Kuznetsova, L. I.; Detusheva, L. G.; Fedotov, M. A.; Likholobov, V. A. Catalytic Properties of Heteropoly Complexes Containing Fe(III) Ions in Benzene Oxidation by Hydrogen Peroxide. *J. Mol. Catal. A: Chem.* **1996**, *111* (1–2), 81–90.

(46) Kuznetsova, L. I.; Detusheva, L. G.; Kuznetsova, N. I.; Fedotov, M. A.; Likholobov, V. A. Relation between Structure and Catalytic Properties of Transition Metal Complexes with Heteropolyanion PW<sub>11</sub>O<sub>39</sub><sup>7-</sup> in Oxidative Reactions. *J. Mol. Catal. A: Chem.* **1997**, *117* (1–3), 389–396.

(47) Jančovičová, V.; Čeppan, M.; Havlínová, B.; Reháková, M.; Jakubíková, Z. Interactions in Iron Gall Inks. *Chem. Pap.* **2007**, *61* (5), 391–397.

(48) Atrián-Blasco, E.; de Cremoux, L.; Lin, X.; Mitchell-Heggs, R.; Sabater, L.; Blanchard, S.; Hureau, C. Keggin-Type Polyoxometalates as Cu(II) Chelators in the Context of Alzheimer's Disease. *Chem. Commun.* **2022**, *58* (14), 2367–2370.

(49) Burgos-Cara, A.; Ruiz-Agudo, E.; Rodriguez-Navarro, C. Effectiveness of Oxalic Acid Treatments for the Protection of Marble Surfaces. *Mater. Des.* **2017**, *115*, 82–92.

(50) Al-Dawsari, A.; Turkustani, A. M.; Bannani, F. Acid-Resistant Corrosion Protection Polyoxometalate Ionic Liquids as Anticorrosion Coatings. *J. Mater. Environ. Sci.* **2019**, *10* (11), 1135–1151.

(51) Santos, F. M.; Brandão, P.; Félix, V.; Domingues, M. R. M.; Amaral, J. S.; Amaral, V. S.; Nogueira, H. I. S.; Cavaleiro, A. M. V. Organic-Inorganic Hybrid Materials Based on Iron(III)-Polyoxotungstates and 1-Butyl-3-Methylimidazolium Cations. *Dalton Trans.* **2012**, *41* (39), 12145–12155.

(52) Duan, Y.; Waerenborgh, J. C.; Clemente-Juan, J. M.; Giménez-Saiz, C.; Coronado, E. Light-Induced Decarboxylation in a Photo-Responsive Iron-Containing Complex Based on Polyoxometalate and Oxalato Ligands. *Chem. Sci.* **2017**, *8* (1), 305–315.

(53) Carrillo, F.; Colom, X.; Suñol, J. J.; Saurina, J. Structural FTIR Analysis and Thermal Characterisation of Lyocell and Viscose-Type Fibres. *Eur. Polym. J.* **2004**, *40* (9), 2229–2234.

(54) Ciolacu, D.; Ciolacu, F.; Popa, V. Amorphous Cellulose - Structure and Characterisation. *Cellul. Chem. Technol.* **2011**, *25*, 13–21.

(55) ISO 1924–2:2008 Paper and Board—Determination of Tensile Properties—Part 2: Constant Rate of Elongation Method (20 Mm/Min); International Organization for Standardization: Geneva, Switzerland, 2008.

(56) ISO 15361:2000 Pulps—Determination of Zero-Span Tensile Strength, Wet or Dry; International Organization for Standardization: Geneva, Switzerland, 2000.

(57) Bodachivskiy, I.; Page, C. J.; Kuzhiumparambil, U.; Hinkley, S. F. R.; Sims, I. M.; Williams, D. B. G. Dissolution of Cellulose: Are Ionic Liquids Innocent or Noninnocent Solvents? *ACS Sustain. Chem. Eng.* **2020**, *8* (27), 10142–10150.

(58) Kosan, B.; Michels, C.; Meister, F. Dissolution and Forming of Cellulose with Ionic Liquids. *Cellulose* **2008**, *15* (1), 59–66.

(59) Ursescu, M.; Măluțan, T.; Cioviță, S. Iron Gall Inks Influence on Papers' Thermal Degradation FT-IR Spectroscopy Applications. *Eur. J. Sci. Theol.* **2009**, *5* (3), 71–84.

(60) Cichosz, S.; Masek, A. IR Study on Cellulose with the Varied Moisture Contents: Insight into the Supramolecular Structure. *Materials* **2020**, *13* (20), 4573–4622.

(61) Łojewska, J.; Lubanska, A.; Łojewski, T.; Miskowicz, P.; Proniewicz, L. M. Kinetic Approach to Degradation of Paper. In Situ FTIR Transmission Studies on Hydrolysis and Oxidation. *e-Preserv. Sci.* **2005**, *2*, 1–12.